Eur. Phys. J. C 28, 297–304 (2003)
Digital Object Identifier (DOI) 10.1140/epjc/s2003-01176-6

THE EUROPEAN PHYSICAL JOURNAL C

A measurement of the photonuclear interactions of 180 GeV muons in iron

The TileCal System of the ATLAS Collaboration

C. Alexa[6], K. Anderson[7], A. Antonaki[3], V. Batusov[9], S. Berglund[20], C. Biscarat[8], O. Blanch[4], G. Blanchot[4], A. Bogush[13], C. Bohm[20], V. Boldea[6], M. Bosman[4], C. Bromberg[10], J. Budagov[9], L. Caloba[19], D. Calvet[8], F. Camarena[23], J. Carvalho[12b], J. Castelo[23], M. V. Castillo[23], M. Cavalli-Sforza[4], V. Cavasinni[15], A. S. Cerqueira[19], M. Cobal[11], F. Cogswell[22], S. Constantinescu[6], D. Costanzo[15], B. Cowan[7], C. Cuenca[23], D. O. Damazio[19], M. David[12a], T. Davidek[16], K. De[2], M. Delfino[4], T. Del Prete[15], B. Di Girolamo[11], S. Dita[6], J. Dolejsi[16], Z. Dolezal[16], A. Dotti[15], R. Downing[22], I. Efthymiopoulos[11], M. Engström[20], D. Errede[22], S. Errede[22], F. Fassi[23], D. Fassouliotis[3], I. Fedorko[5], A. Fenyuk[18], C. Ferdi[8], A. Ferrer[23], V. Flaminio[15], J. Flix[4], E. Fullana[23], R. Garabik[5], V. Garde[8], V. Giakoumopoulou[3], O. Gildemeister[11], V. Gilewsky[13], N. Giokaris[3], A. Gomes[12a], V. Gonzalez[23], S. González De La Hoz[23], V. Grabsky[24], P. Grenier[11], P. Gris[8], V. Guarino[1], C. Guicheney[8], A. Gupta[7], H. Hakobyan[24], M. Haney[22], A. Henriques[11], E. Higon[23], S. Holmgren[20], J. Huston[10], C. Iglesias[4], K. Jon-And[20], T. Junk[22], A. Karyukhin[18], J. Khubua[9,21], S. Kopikov[18], I. Korolkov[4], P. Krivkova[16], Y. Kulchitsky[13,9], P. Kuzhir[14], V. Lapin[18], T. Le Compte[1], R. Lefevre[8], R. Leitner[16], M. Lembesi[3], J. Li[2], M. Liablin[9], Y. Lomakin[9], M. Lokajicek[17], J. M. Lopez Amengual[23], A. Maio[12a], S. Maliukov[9], A. Manousakis[3], C. Marques[12a], F. Marroquim[19], F. Martin[8], E. Mazzoni[15], F. Merritt[7], R. Miller[10], I. Minashvili[9], L. Miralles[4], G. Montarou[8], S. Nemecek[17], M. Nessi[11], L. Nodulman[1], O. Norniella[4], A. Onofre[12c], M. Oreglia[7], A. Pacheco[4], D. Pallin[8], D. Pantea[6], J. Pilcher[7], J. Pina[12a], J. Pinh˜ao[12b], F. Podlyski[8], X. Portell[4], L. E. Price[1], J. Proudfoot[1], R. Richards[10], C. Roda[15], V. Romanov[9], P. Rosnet[8], P. Roy[8], V. Rumiantsau[14], N. Russakovich[9], B. Salvachua[23], E. Sanchis[23], H. Sanders[7], C. Santoni[8], J. G. Saraiva[12a], I. Satsunkevitch[13], L.-P. Says[8], J. Schlereth[1], J. M. Seixas[19], B. Selldèn[20], N. Shalanda[18], P. Shevtsov[14], M. Shochet[7], J. Silva[12a], V. Simaitis[22], A. Sissakian[9], J. Sjölin[20], S. Soares[12a], A. Solodkov[18], O. Solovianov[18], M. Sosebee[2], R. Stanek[1], E. Starchenko[18], P. Starovoitov[14], P. Stavina[5], M. Suk[16], I. Sykora[5], F. Tang[7], P. Tas[16], R. Teuscher[7], S. Tokar[5], N. Topilin[9], J. Torres[23], V. Tsulaia[9], D. Underwood[1], G. Usai[15], S. Valkar[16], M. J. Varanda[12a], A. Vartapetian[2], F. Vazeille[8], I. Vichou[3], V. Vinogradov[9], I. Vivarelli[15], A. White[2], A. Zaitsev[18], T. Zenis[5]

[1] Argonne National Laboratory, Argonne, Illinois, USA
[2] University of Texas at Arlington, Arlington, Texas, USA
[3] University of Athens, Athens, Greece
[4] Institut de Fisica d'Altes Energies, Universitat Autònoma de Barcelona, Barcelona, Spain
[5] Comenius University, Bratislava, Slovakia
[6] Institute of Atomic Physics, Bucharest, Romania
[7] University of Chicago, Chicago, Illinois, USA
[8] LPC Clermont–Ferrand, Université Blaise Pascal / CNRS–IN2P3, Clermont–Ferrand, France
[9] JINR, Dubna, Russia
[10] Michigan State University, East Lansin, Michigan, USA
[11] CERN, Geneva, Switzerland
[12] a) LIP and FCUL Univ. of Lisbon, Portugal
b) LIP and FCTUC Univ. of Coimbra, Portugal
c) LIP and Univ. Católica Figueira da Foz, Portugal
[13] Institute of Physics, National Academy of Sciences, Minsk, Belarus
[14] National Centre of Particles and High Energy Physics, Minsk, Belarus
[15] Pisa University and INFN, Pisa, Italy
[16] Charles University in Prague, Prague, Czech Republic
[17] Institute of Physics, Academy of Sciences of the Czech Republic, Prague, Czech Republic
[18] Institute for High Energy Physics, Protvino, Russia
[19] COPPE/EE/UFRJ, Rio de Janeiro, Brazil
[20] Stockholm University, Stockholm, Sweden
[21] HEPI, Tbilisi State Univ., Tbilisi, Georgia
[22] University of Illinois, Urbana–Champaign, Illinois, USA

[23] IFIC, Centro Mixto Universidad de Valencia-CSIC, E46100 Burjassot, Valencia, Spain
[24] Yerevan Physics Institute, Yerevan, Armenia

Received: 22 January 2003 /
Published online: 5 May 2003 –

Abstract. The energy spectrum and the cross section of photonuclear interactions of 180 GeV muons in iron were measured at the CERN SPS using prototype modules of the ATLAS hadron calorimeter. The differential cross section $(N_A/A)v\mathrm{d}\sigma/\mathrm{d}v$ for a muon fractional energy loss $v = \Delta E_\mu/E_\mu$ was measured in the range $0.1< v <1$. The integrated cross section $(N_A/A)\int_{0.1}^{1} v\mathrm{d}\sigma/\mathrm{d}v$ is $(0.26 \pm 0.03_{\mathrm{stat}} \pm 0.03_{\mathrm{syst}}) \cdot 10^{-6}$ cm^{2}g^{-1} in agreement with the theoretical prediction of $0.267 \cdot 10^{-6}$ cm^{2}g^{-1}. The best adjustment of the data to the theory is achieved for the value of $\sigma_{\gamma N} = (115 \pm 18_{\mathrm{stat}} \pm 15_{\mathrm{syst}})\mu$b of the photon-nucleon cross section for photons with energies in the range from 18 to 180 GeV.

1 Introduction

Photonuclear interactions of muons $\mu + A \rightarrow \mu^{'} + hadrons + X$ were first observed [1] in 1955. Despite the fact that the cross section is relatively large, very few measurements of muon photonuclear reactions at low momentum transfer have been reported [2,3]. This mechanism of muon energy loss has an increasing impact on the design and the analysis of several type of new experiments, and needs a better understanding.

In Large Hadron Collider (LHC) experiments, high-energy muons are involved in a broad variety of new physics processes. They traverse substantial lengths of dense materials, and their experimental signature must be thoroughly understood in order to identify them, measure their energy and to take the hadronic showers accompanying muon tracks properly into account in the energy flow. In underground experiments, photonuclear interactions of muons must also be taken precisely into account because they may produce backgrounds to rare signals [2].

This paper describes a measurement of muon photonuclear interactions in iron performed in 1998 using 180 GeV/c positive muons incident to a prototype module of the ATLAS [4] Tile Calorimeter [5].

As pointed out in [6], two separate theoretical predictions lead to very different expectations: in particular the more recent prediction of Bezrukov and Bugaev [7] is about an order of magnitude larger than the results based on [8,9]. Supported by the results of [2], the prediction of [7] is compared to the experimental results described in this paper.

2 Experiment and data analysis

The ATLAS Tile Calorimeter is an iron-scintillator sampling calorimeter equipped with wavelength-shifting fibre readout. An important feature of this calorimeter is that the scintillator tiles are placed perpendicular to the colliding beams; a detailed description of the calorimeter concept is given elsewhere [5]. The experimental set-up is shown in Fig. 1. Here, the muon beam crossed the scintillator tiles of a 5.6 m long prototype module of the Tile calorimeter at perpendicular incidence, entering the center

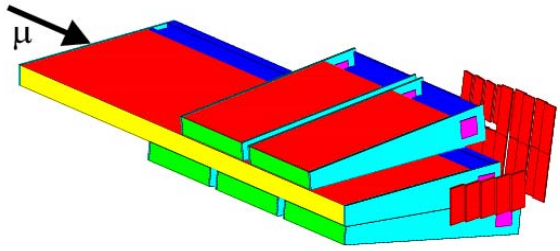

Fig. 1. The experimental setup. As indicated by the arrow, the muon beam impinges centrally on one side of the 5.6 m long ("large") calorimeter module. At the downstream end three smaller modules were placed below the large module and two were placed above it

of the side facing the beam. For purposes of shower containment and data selection, five smaller modules, each spanning 1 m along the beam direction, sandwiched the large module at the downstream end; three modules were placed below and two above the large module. Data were taken with this set-up on the H8 beam of the CERN SPS.

In this configuration the muon beam traversed a fully periodic structure consisting of alternating slabs of iron (14 mm), scintillator (3 mm) and about 0.4 mm of other light elements (scintillator wrappings, glue). The fibres collecting light from the scintillator are grouped into readout cells that segment the calorimeter module along the beam direction and perpendicular to it in the horizontal plane. Along the direction of the incident particles sixteen cells are traversed, each consisting of 17 to 21 iron-scintillator periods. The segmentation of the small modules is similar but the readout cells are smaller and consist of 11 or 12 periods.

Particles of the momentum-analysed muon beam, with a mean momentum $p_\mu = 180$ GeV/c, triggered a coincidence of three scintillator hodoscopes; the direction of incidence being measured by a pair of two-coordinate wire chambers. Approximately 400 000 muon triggers were used in this analysis.

A minimum-ionizing particle (*mip*) signal was required in the scintillator hodoscopes to suppress triggers with more than one incident particle. Only events within a beam spot of 1.5×1.5 cm^2 defined by the beam chambers were selected. This cut reduced the momentum spread of the selected particles. In order to eliminate the low-level

hadron and electron contamination of the muon beam, the signal in each of the first five calorimeter cells was required to be compatible with that of a *mip*. With this cut, only particles traversing 7.5 nuclear interaction lengths or 80 radiation lengths without showering were selected; this left less than 0.5 events due to hadron-induced interactions in the analysed data sample. The contribution from muon decay-in-flight events inside the calorimeter and within the acceptance region is estimated to be 1.5 events in the selected data sample. Two events without a muon escaping the shower were found and excluded from the analyzed sample. As a result of these cuts about $N_{tot} = 190\ 000$ events were selected for further analysis.

2.1 Selection of photonuclear events

Only events with the largest signal occurring in the 7th to the 13th of the 16 cells altogether traversed by muons are selected. This assures optimal containment of showers produced by muon photonuclear interactions. This defines a region of 124 iron-scintillator periods in which muon photonuclear interaction are accepted.

The photonuclear candidates were selected by requiring significant transverse leakage of the shower from the large module, typical of hadronic showers. Specifically, at least 0.75 GeV in one of a cell of the five small calorimeters sandwiching the large module were required.

The longitudinal location $z_{\rm small}$ of the shower maximum in the small calorimeters is clearly correlated with the location of the shower maximum in the large calorimeter $z_{\rm large}$ as shown in Fig. 2. To reduce the background from cosmic rays and electronic noise in the small calorimeters the difference $z_{\rm small} - z_{\rm large}$ was required to be within ± 700 mm of the measured mean value of 500 mm (see Fig. 2).

The energy ΔE_μ lost by muons in the calorimeter modules is calculated excluding the minimum-ionization signal. It was obtained summing the signals of five consecutive cells of the large calorimeter (around the cell with the largest signal) to the signals in the small calorimeters and subtracting the value of the truncated mean of the muon signal in the cells traversed by muons. The latter mean equals $1.7 \cdot E_{\rm mp}$ where $E_{\rm mp}$ is the most probable value of the muon ionization energy loss for each cell.

The energy scale of the calorimeters was calibrated using electron beams, and has an uncertainty of $\pm 2\%$. The measured value of ΔE_μ^{meas} (in GeV) was corrected using the relation:

$$\Delta E_\mu = \frac{e/h}{1 + (e/h - 1)0.11 ln(\Delta E_\mu^{meas})} \Delta E_\mu^{meas},$$

where $e/h = 1.35 \pm 0.05$ as measured with the Tile Calorimeter [5]. The muon fractional energy loss v is given by $v = \Delta E_\mu/(E_\mu - \epsilon)$, subtracting the measured muon energy loss upstream of the shower, ϵ, from the nominal beam energy.

Acceptance and background considerations, given in detail later in the paper, led to selecting for analysis of events with $v \geq 0.1$ giving a sample of 79 photonuclear interactions candidates. A typical candidate is shown in Fig. 3, together with an event in which an electromagnetic shower is produced by the muon. The latter type of events is the main source of background, as will be discussed next.

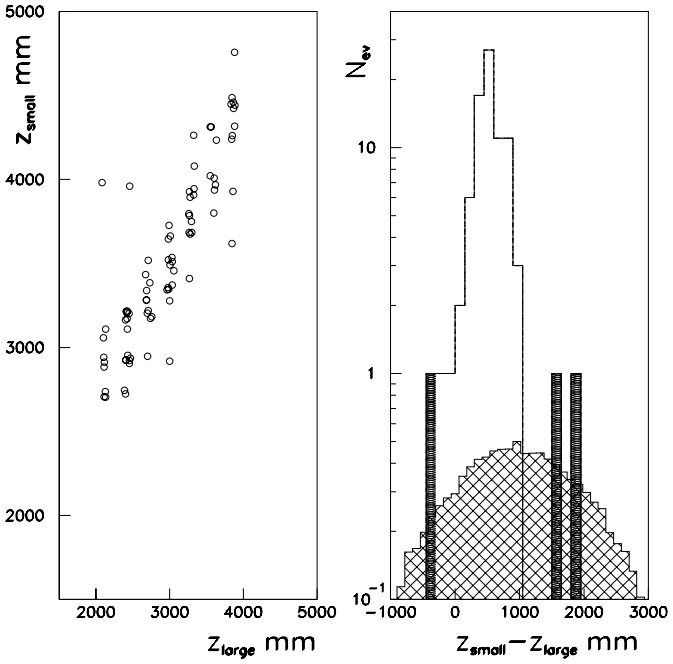

Fig. 2. The left plot shows the correlation of the longitudinal locations of showers maxima in the large ($z_{\rm large}$) and small ($z_{\rm small}$) calorimeter modules. The measured distribution of the difference $z_{\rm small} - z_{\rm large}$ is shown by the line histogram in the *right plot*. The expected distribution of this difference from events with radiative or knock-on muon energy losses with cosmic rays signals in the small calorimeters is shown by the cross-hatched histogram. Three events (*full histogram*) have been excluded from the analysis

2.2 Acceptance

The acceptance for photonuclear processes is limited by the requirement that some shower energy is detected in the small calorimeters. Due to the constant threshold of 0.75 GeV the acceptance is smaller for the lower-energy showers, or equivalently for small v.

Kinematically, hadrons produced in photon–nucleus interactions are extremely similar to those produced in pion–nucleus interactions. This is shown in Fig. 4, which compares the total energy and the scalar transverse energy sums of particle produced by photons and pions on nucleons, as calculated with PYTHIA 5.7 [11] for 54 and 180 GeV photons and pions. This observation makes it possible to calculate the acceptance of photon–nucleus interactions in this experiment, based on the lateral distribution of pion showers observed in the same test beam. However the available pion data are at angles of incidence different than that of the muon beam, hence the following less direct procedure was used.

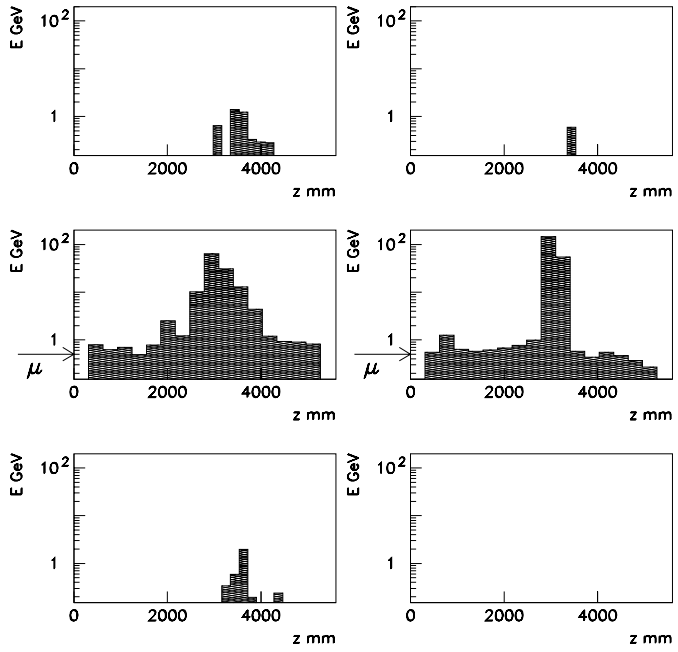

Fig. 3. Examples of a photonuclear interaction of a muon (*left plots*) and of a background event (*right plots*). The signals in the cells of the small modules (*top* and *bottom plots*) and in the large calorimeter module (*center plots*) are shown. The photonuclear interactions are characterized by longer and broader showers compared to the background events. The incoming muon direction is indicated by the arrow

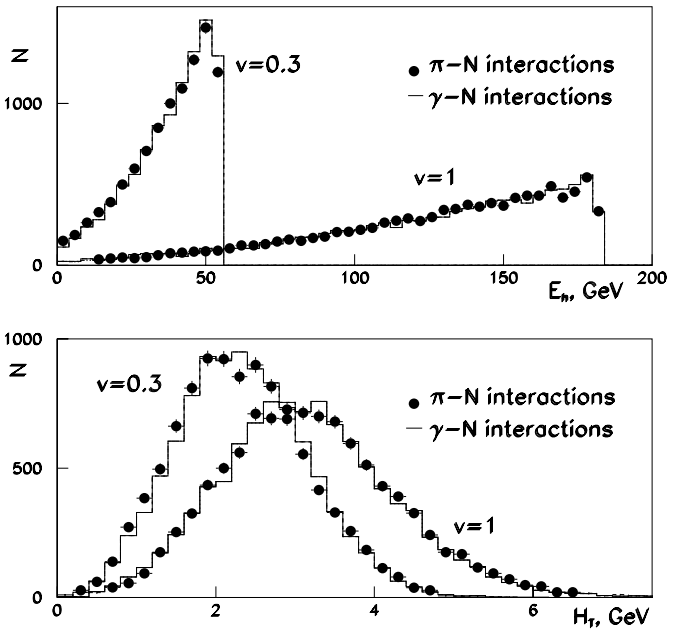

Fig. 4. PYTHIA simulations of pion and gamma interactions with nucleons. Results for energies corresponding to the values of v =0.3 and v =1 are shown. Top plot: distribution of total energy E_h carried by secondary hadrons produced in gamma–nucleon interactions (*histograms*) and in pion–nucleon interactions (*full circles)*. Bottom plot: distributions of the scalar sum $H_T = \Sigma|\mathbf{p_T}|$ of transverse momenta of secondary hadrons

The acceptance was calculated using available pion beam data and GEANT [10] simulations with the GCALOR [12] hadronic interactions code. The pion beam data were taken at energies of E_π = 20, 50, 100, 150 and 180 GeV (the corresponding values of v are $v = E_\pi/180$), and with beams impinging on the calorimeters at several angles θ between 50^0 and 80^0 to the muon direction shown in Fig. 1. Using these data, the acceptance $acc_\pi(\theta, v)$ for pion showers giving signals of 0.75 GeV or more in at least one cell of the small modules was obtained. Acceptance values obtained by simulations, $acc_{MC}(\theta, v)$, and with data, $acc_\pi(\theta, v)$, are in agreement within 10%. Finally, pion–induced showers with the same longitudinal distribution along z as the candidate photonuclear events, and in the direction of muons, were simulated and the acceptance $acc_{MC}(z, v)$ was calculated, again taking advantage of the observed similarity of photon–nucleus and pion–nucleus interactions. These values were corrected by the ratio of $acc_\pi(\theta, v)$ and $acc_{MC}(\theta, v)$ to find the acceptances $acc(v)$ used in this analysis:

$$acc(v) = \langle acc_{MC}(z, v)\rangle \cdot \left\langle \frac{acc_\pi(\theta, v)}{acc_{MC}(\theta, v)} \right\rangle .$$

In the expression, the first mean value in angular brackets is taken over the z positions of the generated pion showers, the second mean is taken over all available pion incident angles θ.

The values of the acceptance are shown in bottom plot of Fig. 5 together with the parametrization $acc(v) = 1.225 \cdot v - 0.4025 \cdot v^2$, which was used to evaluate the cross sections. A systematic uncertainty of ±10% in the acceptance was estimated from the comparison of pion data and simulations. Another source of systematic errors is the effect on 0.75 GeV cut due to the 2% uncertainty of the calorimeter energy scale. This leads to an additional systematic uncertainty in the acceptance of 5% and 1% at v=0.1 and v=1 respectively.

2.3 Backgrounds

The main signature of a photonuclear event is the presence of energy in at least one of the small calorimeter cells. Three possible sources of background leading to a signal in excess of 0.75 GeV in these cells can be identified:
Electronic noise. The typical r.m.s. value of electronic noise in the small calorimeter cells is 20 MeV, hence the probability to produce a signal greater than 0.75 GeV should be negligible.
Cosmic rays and beam halo particles. The charge signal from the small calorimeters is integrated over a 200 ns gate, warranting a detailed estimate of the effect of such random coincidences.
Lateral leakage of electromagnetic showers. Electromagnetic showers produced in the large module by knock-on electrons or radiative losses of muons, and leaking into the small modules are the main source of background to photonuclear processes. The transverse dimension of about 12 Moller radii does not completely suppress electromagnetic

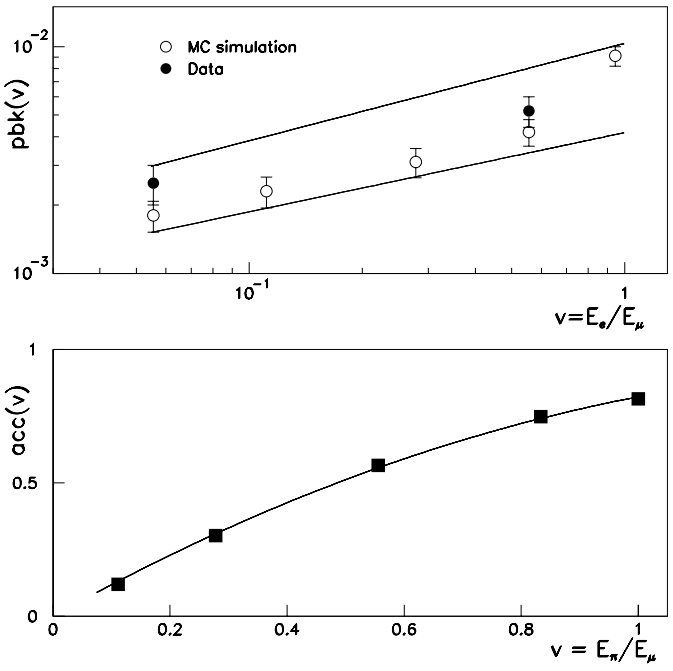

Fig. 5. Top plot: the electromagnetic showers background $pbk(v)$ estimated with the electron beams (*full circles*) and with Monte Carlo simulations. Bottom plot: the acceptance of photonuclear events estimated with hadron beams of different energies E_π. The curve is the parametrization described in the text

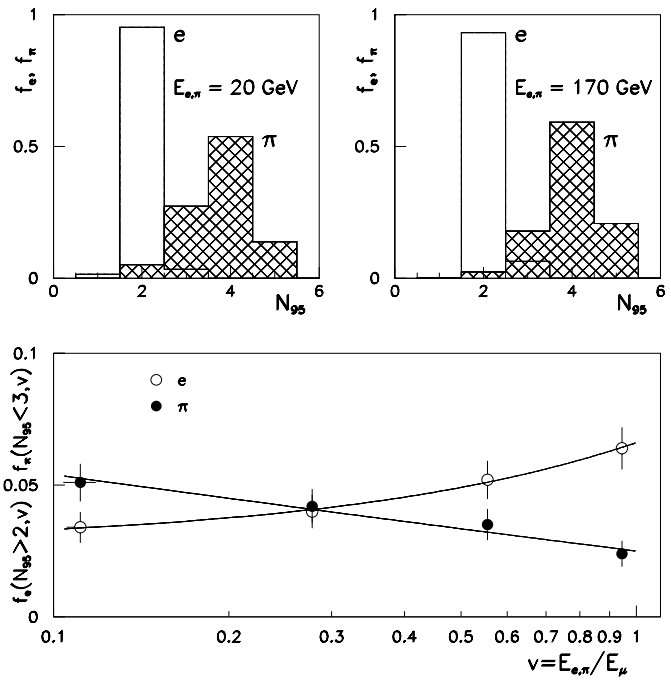

Fig. 6. Monte Carlo study of electromagnetic and hadronic showers separation using the variable N_{95} defined in the text. The two upper plots show the distribution of N_{95} for simulated electron and pion showers with energies of 20 and 170 GeV. Bottom plot: the fraction $f_e(N_{95} > 2, v)$ of electron showers with $N_{95} > 2$ for different electron energies, and the fraction $f_\pi(N_{95} < 3, v)$ of pion showers with $N_{95} < 3$

leakage out of the large calorimeter because radiation may leak through the scintillator tiles.

All events with a *mip* signal in the large calorimeter were used to estimate the background due to cosmic rays, beam halo and any unexpected electronic noise. It was found that only a fraction of 10^{-3} of such events is accompanied by a signal exceeding 0.75 GeV in at least one small calorimeter cell.

Data taken with electron beams impinging on the 5.6 m module from the direction opposite to that of the muon beam (*i.e.* hitting the side nearest to the small modules) were used to find the probability that lateral electromagnetic shower leakage exceeds 0.75 GeV in the small modules, that is $1.5{\cdot}10^{-3}$ and $4{\cdot}10^{-3}$ with 10 and 100 GeV electrons respectively. To obtain this leakage probability for several energies, the electromagnetic showers were simulated using GEANT and reproducing starting points, lateral and angular positions in accord with the data. The results including the energy independent probability of 10^{-3} are shown in the upper plot of Fig. 5, where the estimated error band is also shown.

In summary, the probability $pbk(v)$ of observing a fake photonuclear event in this analysis can be parametrized by the band indicated in upper plot of Fig. 5.

An alternative manner to deal with these backgrounds is to directly remove such events taking advantage of the different longitudinal profiles of electromagnetic and hadronic showers, observed using the longitudinal segmentation of the large calorimeter. A Monte Carlo simulation of the distribution of the smallest number N_{95} of adjacent cells containing at least 95% of the shower energy deposited in five adjacent cells is shown in Fig. 6. It is seen that an overwhelming fraction of electromagnetic showers deposit 95% of the energy in less than three calorimeter cells ($N_{95} \leq 3$), whereas for hadronic showers $N_{95} \geq 3$ with the most probable value $N_{95} = 4$.

The distributions of the variable N_{95} for photonuclear interaction candidates shown in the top plots of Fig. 7 clearly indicate that the candidate sample consists almost entirely of hadronic showers. Eliminating events with $N_{95} < 3$ is an effective background cut. The inefficiency associated to this cut was estimated using the Monte Carlo results in Fig. 6, which were parametrized by $f_\pi(N_{95} < 3, v) = 0.310 \cdot v^{-0.039} - 0.285$. The remaining contamination of the selected sample by electromagnetic showers is <1% and is taken into account in the estimate of systematic errors.

The results of the two background estimates are compared in the bottom plot of Fig. 7, where the band corresponds to the $pbk(v)$ calculated above and the points are the events eliminated based on the value of N_{95}, per bin of $\Delta v = 0.1$. More specifically the band is obtained by multiplying the upper and lower limits of $pbk(v)$ by the number of muon events with electromagnetic energy losses $N_{em}(v)$, which is obtained from the theoretical expressions of knock-on, bremsstrahlung and pair production cross sections given in [13,14] and scaled to N_{tot} muons.

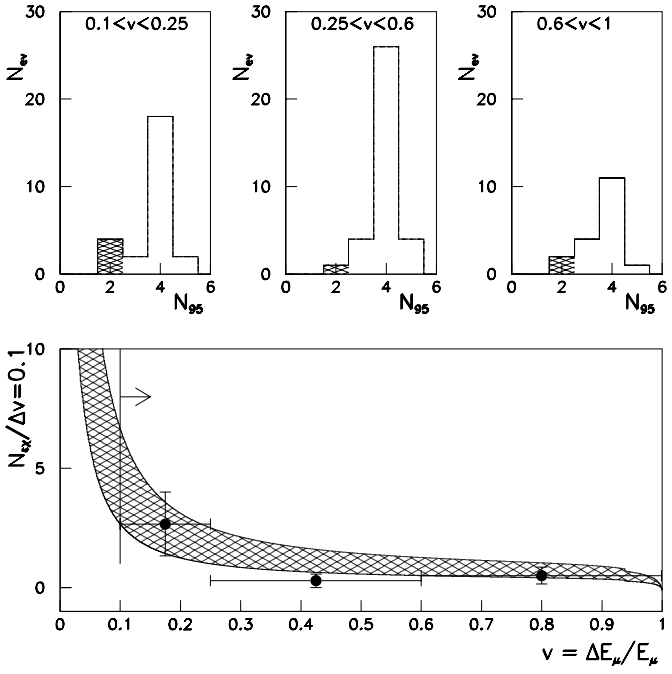

Fig. 7. Top plots: the distribution of the variable N_{95} described in the text for photonuclear event candidates, in three different intervals of v. Hatched events with the value of N_{95}=2, which is typical of electromagnetic showers, have been excluded from the analysis. Bottom plot: comparison of the number of events with $N_{95} = 2$ per bin of 0.1 in v (*filled circles*) with the calculated number of background events from the three sources of background examined (*cross-hatched band*)

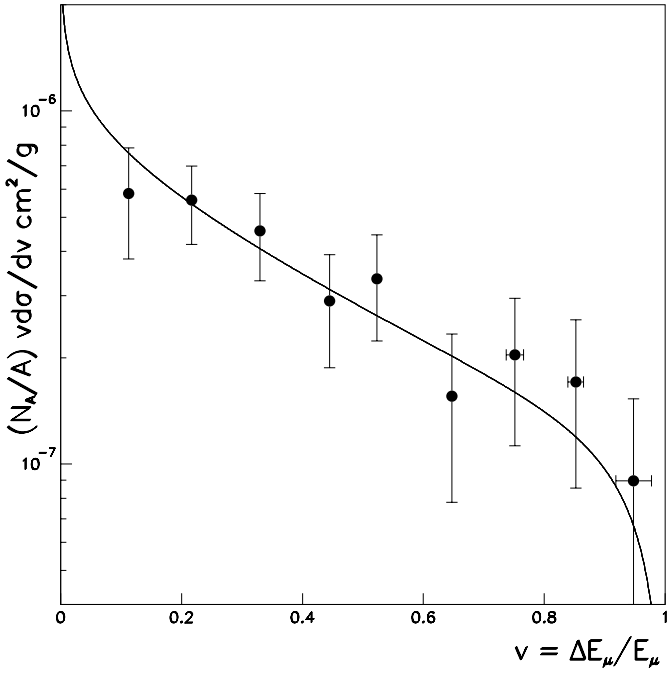

Fig. 8. The full circles show the measured differential energy-loss probability spectrum of 180 GeV muons by photonuclear interactions in iron. The curve is the theoretical prediction of [7]. The errors shown are statistical only

The good agreement of the two background estimates over the observed range of energy losses gives confidence in the purity of the photonuclear event sample. Figure 7 also shows that for $v < 0.1$ the background rapidly grows, which motivates the choice of $v > 0.1$ in this analysis.

2.4 Evaluation of the cross section

The differential probability of fractional energy loss v per g/cm^2 of iron was calculated in nine equal intervals $\Delta v_i (i = 1, ..., 9)$ of v using only events with $N_{95} \geq 3$. The following expression is used:

$$\frac{N_A}{A_{Fe}} v \frac{\mathrm{d}\sigma}{\mathrm{d}v} = \frac{\sum_{j=1}^{N_i} v_j \cdot w(v_j)}{N_{tot} \Delta v_i} \frac{1}{L_{Fe} \cdot \rho_{Fe}} \times \frac{1}{1 + L_{sci}\rho_{sci}/L_{Fe}\rho_{Fe}},$$

where each event j has weight $w(v_j) = 1/[1 - f_\pi(N_{95} < 3, v_j)]acc(v_j)$ with $f_\pi(N_{95} < 3, v_j)$ and $acc(v_j)$ defined above. The variable v_j is the measured value of v for the j-th event within the i-th interval of v; N_i is the number of events in the i-th interval, N_{tot} is the total number of selected primary muons, Δv_i is the width of the i-th interval. N_A is the Avogadro number in units of mol^{-1}, and L_{Fe}, ρ_{Fe} and A_{Fe} are the length of the accepted region of the iron in cm, its density in g·cm^{-3} and atomic weight of the iron in g·mol^{-1} respectively. The length and the density of light materials (mainly the scintillator) are denoted by L_{sci}, ρ_{sci}. The correction $L_{sci}\rho_{sci}/L_{Fe}\rho_{Fe}$ due to the contribution of light materials is 3%.

The values of $(N_A/A)v\mathrm{d}\sigma/\mathrm{d}v$ are given in Table 1 and shown in Fig. 8.

An other evaluation of the probability of fractional energy loss v can be made using the same expression as above but without removing the candidate events with $N_{95} < 3$. Now the weight of each event is

$$w(v_j) = \frac{1 - N_{em}(v_i) \cdot pbk(v_j)/N_i}{acc(v_j)}$$

where the term subtracted form 1 is the probability that an event comes from backgrounds.

The cross-section (or energy-loss probability) values obtained with this second method are 2% higher than in the first calculation, which led to an estimate of a further 2% systematic uncertainty.

2.5 Systematic errors

The systematic errors of the energy loss probability spectrum are dominated by the uncertainty of the acceptance. The uncertainty of ±0.05 in the e/h ratio and the 2% uncertainty in the energy scale together lead to an uncertainty in the cross section that does not exceed ±5% over the range of v. The error in the thickness of the absorber plates is about 1%.

The overall systematic error is ±12% with very weak energy dependence from the value of 12.5% at v=0.1 to 11.5% at v close to 1. The individual contributions to this value are listed in the following table:

Source of systematic uncertainty	Syst. error in %	
	$v \to 0.1$	$v \to 1$
Acceptance	±10	±10
Energy scale in small calorimeters	±5	±1
Cut $N_{95} \geq 3$	−1	−1
Background subtraction	+2	+2
e/h and energy scale	±5	±5
Absorber thickness	±1	±1
Total	±12.5%	±11.5%

3 Comparison with theory

The experimental results on photonuclear energy losses in iron are compared in Fig. 8 and Table 1 to the theoretical prediction of Bezrukov and Bugaev [7], as given in [15]:

$$\left(v\frac{\mathrm{d}\sigma}{\mathrm{d}v}\right)_{\text{photonuclear}} = \frac{\alpha}{2\pi}A_{Fe}\sigma_{\gamma N}(\Delta E_\mu)v^2\Gamma(E_\mu, v)$$

The form $vd\sigma/dv$ is chosen because it is not divergent at $v = 0$. In the formula, α is the fine-structure constant and $\sigma_{\gamma N}(\Delta E_\mu) = 114.3 + 1.647\ln^2(0.0213\Delta E_\mu[\mathrm{GeV}])\ \mu b$ is the parametrization of the photon-nucleon cross section for the energy loss $\Delta E_\mu = vE_\mu$. The function $\Gamma(E_\mu, v)$ is given by (m_μ is the muon mass):

$$\begin{aligned}\Gamma(E_\mu, v) = {} & \frac{3}{4}G(x)\left(\kappa\ln\left(1+\frac{m_1^2}{t}\right) - \frac{\kappa m_1^2}{m_1^2+t} - \frac{2m_\mu^2}{t}\right) \\ & + \frac{1}{4}\left(\kappa\ln\left(1+\frac{m_2^2}{t}\right) - \frac{2m_\mu^2}{t}\right) \\ & + \frac{m_\mu^2}{2t}\left(\frac{3}{4}G(x)\frac{m_1^2}{m_1^2+t} + \frac{1}{4}\frac{m_2^2}{t}\ln\left(1+\frac{t}{m_2^2}\right)\right)\end{aligned}$$

with

$$G(x) = \frac{3}{x^2}\left(\frac{x^2}{2} - 1 + e^{-x}(1+x)\right),$$

$$x = 0.00282A_{Fe}^{1/3}\sigma_{\gamma N}(\Delta E_\mu),\ t = \frac{m_\mu^2 v^2}{1-v},$$

$$\kappa = 1 - \frac{2}{v} - \frac{2}{v^2},\ m_1^2 = 0.54\ \mathrm{GeV}^2,\ m_2^2 = 1.80\ \mathrm{GeV}^2.$$

The results and the theoretical prediction are in good agreement. The integrated value of the theoretical $vd\sigma/dv$ for $v > 0.1$ is 71% of the total. The experimental value $(0.26 \pm 0.03_{\text{stat}} \pm 0.03_{\text{syst}}) \cdot 10^{-6}\ \mathrm{cm}^2\mathrm{g}^{-1}$ of the integral $(N_A/A)\int_{0.1}^{1} v\mathrm{d}\sigma/\mathrm{d}v$ is also in very good agreement with the theoretical prediction of $0.267 \cdot 10^{-6}\ \mathrm{cm}^2\mathrm{g}^{-1}$. The results of this experiment together with those of [2] support the theoretical description of muon photonuclear interactions given by [7].

Table 1. The measured differential cross section values $(N_A/A)v\mathrm{d}\sigma/\mathrm{d}v$ for fractional photonuclear muon energy losses v and theoretical predictions [7]. First errors are statistical and second are systematic

$\langle v\rangle$	$(N_A/A)v\mathrm{d}\sigma/\mathrm{d}v$(meas.) $\mathrm{cm}^2\cdot\mathrm{g}^{-1}$	$(N_A/A)v\mathrm{d}\sigma/\mathrm{d}v$(th.) $\mathrm{cm}^2\cdot\mathrm{g}^{-1}$
0.113 ± 0.009	$(0.58 \pm 0.20 \pm 0.07) \times 10^{-6}$	0.76×10^{-6}
0.217 ± 0.006	$(0.56 \pm 0.14 \pm 0.06) \times 10^{-6}$	0.57×10^{-6}
0.33 ± 0.01	$(0.46 \pm 0.13 \pm 0.05) \times 10^{-6}$	0.41×10^{-6}
0.45 ± 0.01	$(0.29 \pm 0.10 \pm 0.03) \times 10^{-6}$	0.31×10^{-6}
0.52 ± 0.01	$(0.33 \pm 0.11 \pm 0.04) \times 10^{-6}$	0.26×10^{-6}
0.65 ± 0.01	$(0.16 \pm 0.08 \pm 0.02) \times 10^{-6}$	0.20×10^{-6}
0.75 ± 0.01	$(0.20 \pm 0.09 \pm 0.03) \times 10^{-6}$	0.16×10^{-6}
0.85 ± 0.01	$(0.17 \pm 0.08 \pm 0.02) \times 10^{-6}$	0.12×10^{-6}
0.95 ± 0.03	$(0.09 \pm 0.06 \pm 0.01) \times 10^{-6}$	0.07×10^{-6}

The main scale factor in the theoretical formula is the value of the photon-nucleon cross section $\sigma_{\gamma N}$. In the studied energy region it varies very slowly with the energy. The predicted values, using the parametrization given above, are 116 μb and 117 μb for v =0.1 and v =1 respectively. The parametrization is valid up to the highest energies of the HERA collider, where the measured values of 143±4μb [16] and $165 \pm 11\mu$b [17] are in good agreement with the value of 157 μb predicted by the parametrization used in the theoretical formula for a mean value of $\sqrt{s}$ =200 GeV.

These experimental results can alternatively be used to measure $\sigma_{\gamma N}$. For this purpose the measured cross section is fitted using $\sigma_{\gamma N}$ as a free parameter. The best agreement with the theory is obtained for
$\sigma_{\gamma N} = (115 \pm 18_{\text{stat}} \pm 15_{\text{syst}})\mu$b for photons from 18 to 180 GeV ($\sqrt{s}$ from 6 to 18 GeV).

Acknowledgements. We sincerely thank the technical staffs of the collaborating Institutes for their important and timely contributions. Financial support is acknowledged from the funding agencies of the collaborating Institutes. We are grateful to the staff of the SPS, and in particular to K. Elsener, for the excellent beam conditions and assistance provided during our tests. Finally we thank the members of the former RD13 collaboration for providing and supporting the Data Acquisition system.

References

1. E.P. George, J. Evans, Proc. Phys. Soc. **68**, 829 (1955)
2. G. Battistoni et al., hep-ex/9809006, 9 Sep 1998; E. Scapparone for the MACRO Collaboration, 10^{th} Int. Symp. on Very High Energy Cosmic Ray Interactions, 1998, hep-ex/9902016, 15 Feb 1999, published in Nucl. Phys. B, Proc. Suppl. **75A**, 397 (1999)

3. P.L. Jain et al., Phys. Rev. D **7**, 3248, 1973; K. Honda et al., Proc. Int. Conf. Cosmic Rays, Kyoto, 10, 226, 1979; C. Grupen, Tokyo Univ. preprint SI-81-22, Nov. 1981
4. ATLAS Collaboration, ATLAS Technical Proposal, report CERN/LHCC/94–43
5. F. Ariztizabal et al., Nucl. Instrum. Methods A **349**, 384 (1994); E. Berger et al., report CERN/LHCC 95–44; Atlas Collaboration, Tile Calorimeter TDR, CERN/LHCC 96-42
6. G. Battistoni et al., Nucl. Instrum. Methods A **394**, 136 (1997)
7. L.B. Bezrukov, E.V. Bugaev, Sov. J. Nucl. Phys. **33**, 635 (1981)
8. H. Fesefeldt, preprint PITHA 85/02, Aachen 1985
9. M. Nagano, preprint INSJ-120, Institute for Nuclear Study, Tokyo University, 1970
10. R. Brun et al., CERN GEANT User's guide, DD/EE 84-1 (1992)
11. T. Sjostrand, PYTHIA 5.7 and JETSET 7.4 Physics and Manual, CERN-TH.7112/93, CERN 1993
12. C. Zeitnitz, T.A. Gabriel, Nucl. Instrum. Methods A **349**, 106 (1994)
13. E. Berger et al., Z. Phys. C **73**, 455 (1997)
14. P. Amaral et al., Eur. Phys. J. C **20**, 487 (2001)
15. W. Lohmann et al., CERN report 85–03 (1985)
16. ZEUS Coll. (M. Derrick et al.), Z. Phys. C **63**, 391 (1994)
17. H1 Coll. (S. Aid et al.), Z. Phys. C **69**, 27 (1995)